HHS Public Access

Author manuscript

Cancer Discov. Author manuscript; available in PMC 2016 April 01.

Published in final edited form as:

Cancer Discov. 2015 October ; 5(10): 1058–1071. doi:10.1158/2159-8290.CD-15-0370.

Detection of Enhancer-Associated Rearrangements Reveals Mechanisms of Oncogene Dysregulation in B-cell Lymphoma

Russell J.H. Ryan[1,3,*], **Yotam Drier**[1,3,*], **Holly Whitton**[3], **M. Joel Cotton**[1,3], **Jasleen Kaur**[1,3], **Robbyn Issner**[3], **Shawn Gillespie**[1,3], **Charles B. Epstein**[3], **Valentina Nardi**[1], **Aliyah R. Sohani**[1], **Ephraim P. Hochberg**[2], and **Bradley E. Bernstein**[1,3]

[1]Department of Pathology, Massachusetts General Hospital and Harvard Medical School

[2]Department of Medicine, Massachusetts General Hospital and Harvard Medical School

[3]Broad Institute of Harvard University and MIT

Abstract

B-cell lymphomas frequently contain genomic rearrangements that lead to oncogene activation by heterologous distal regulatory elements. We utilized a novel approach, termed 'Pinpointing Enhancer-Associated Rearrangements by Chromatin Immunoprecipitation' or PEAR-ChIP, to simultaneously map enhancer activity and proximal rearrangements in lymphoma cell lines and patient biopsies. This method detects rearrangements involving known cancer genes, including *CCND1*, *BCL2*, *MYC*, *PDCD1LG2*, *NOTCH1*, *CIITA*, and *SGK1*, as well as novel enhancer duplication events of likely oncogenic significance. We identify lymphoma subtype-specific enhancers in the *MYC* locus that are silenced in lymphomas with *MYC*-activating rearrangements and are associated with germline polymorphisms that alter lymphoma risk. We show that *BCL6*-locus enhancers are acetylated by the *BCL6*-activating transcription factor MEF2B, and can undergo genomic duplication, or target the *MYC* promoter for activation in the context of a "pseudo-double-hit" t(3;8)(q27;q24) rearrangement linking the *BCL6* and *MYC* loci. Our work provides novel insights regarding enhancer-driven oncogene activation in lymphoma.

Keywords

Lymphoma; Rearrangement; Enhancer; BCL6; MYC

Introduction

Genomic rearrangements represent an important oncogenic mechanism in human cancers. Rearrangements occurring within genes may produce fusion transcripts encoding chimeric proteins with novel functions. In contrast, many recurrent translocations in B-cell lymphomas, such as those involving *BCL2*, *CCND1*, and frequently *MYC*, result in high-level expression of intact oncogene coding transcripts from their native promoters. Aberrant

Please address correspondence to: Bradley E. Bernstein, MD, PhD, Department of Pathology, Massachusetts General Hospital, Simches Research Ctr., 185 Cambridge St., Boston, MA 02114, Bernstein.Bradley@mgh.harvard.edu, Phone: 617-643-3559.

*These authors contributed equally to this work

The authors disclose no potential conflicts of interest.

oncogene expression in these events is thought to be dependent on looping interactions between the oncogene promoter and cis-regulatory elements (enhancers) from the translocation partner locus, often *IGH* (1). The identification of recurrent "enhancer hijacking" translocations (2) and enhancer amplification events (3) in non-lymphoid cancers suggests that this may be a common oncogenic mechanism, and raises the need for improved methods for genome-wide detection and functional characterization of such events.

Enhancers are non-coding regulatory elements that stimulate transcription through looping-mediated interactions with promoters, and are activated in specific cellular contexts by different combinations of sequence-specific transcription factors (TFs). Active enhancers adopt a signature chromatin structure, and can be identified by mapping histone H3 Lys27 acetylation (H3K27ac) via chromatin immunoprecipitation and high-throughput sequencing (ChIP-Seq) (4,5). Strong histone acetylation is a common feature of genomic loci that undergo recurrent physiologic or oncogenic immunoglobulin gene rearrangements in B-cell lymphoma (6,7).

Here we describe PEAR-ChIP (Pinpointing Enhancer-Associated Rearrangements by Chromatin Immunoprecipitation and Paired-end sequencing), a novel approach that combines H3K27ac ChIP-Seq with paired-end sequencing analysis to map genomic rearrangements involving acetylated regulatory elements. Investigating a panel of 14 primary patient biopsies and 8 cell line models representing multiple classes of B-cell lymphoma, we identify known and novel rearrangements, and gain insight into the mechanisms by which these translocations exploit native regulatory circuits to drive activation of *MYC*, *BCL6* and other oncogenes.

Results

Identification of oncogenic rearrangements in mantle cell lymphoma by PEAR-ChIP

Histone H3K27ac ChIP-Seq is a powerful tool for genome-wide identification of active enhancers, but identifying relationships between enhancers and genomic rearrangements has required addition of a second sequencing technology, such as whole-genome sequencing (WGS) (2). However, we reasoned that analysis of paired-end sequencing data from H3K27ac ChIP-Seq libraries could efficiently detect rearrangements involving enhancers, as long as the breakpoints occurred within acetylated elements (Fig. 1A).

We first tested this approach in mantle cell lymphoma (MCL), a poor-prognosis lymphoma characterized by reciprocal translocations between the *IGH* J recombination region on chromosome 14 and a >300 kb gene-free region upstream of the *CCND1* gene on chromosome 11, with half of cases showing breakpoint within a major translocation cluster (MTC) (8).

We performed H3K27ac ChIP-seq with paired-end sequencing on frozen tissue from four primary MCL tumor biopsies (see Supplementary Table S1 for clinical and diagnostic details about all samples) and four MCL cell lines. All cases showed strong H3K27ac signal extending from the *IGH* μ intronic enhancer and covering the J recombination region. In each case, we identified sequencing read pairs that spanned the t(11;14) rearrangement

breakpoint, allowing for precise breakpoint identification (Fig. 1A, 1B). Chromosome 11 breakpoints were visible in H3K27ac ChIP-Seq tracks as 'spikes' of acetylation signal in the gene desert upstream of *CCND1*. In four MCL cases, atypical read pairing also identified a focal deletion or inter-chromosomal rearrangement resulting in partial deletion of the *CCND1* 3' UTR, a recurrent event in MCL that increases stability of the *CCND1* transcript by eliminating a microRNA binding site, and is associated with a more aggressive disease course (9). In all eight cases, we also detected productive VDJ recombination of the alternate *IGH* allele not affected by the t(11;14) (Fig. 1A, Supplementary Table S2).

To establish the genome-wide PEAR-ChIP method, we adapted dRanger and BreakPointer (10), originally developed for detecting rearrangements in WGS data, to scan paired-end H3K27ac ChIP-Seq data for genomic alterations. In the MCL line Rec-1, PEAR-ChIP detected a truncating deletion of *NOTCH1*, recently shown to be an activating oncogenic event (11). In the MCL line Jeko-1, we detected a rearrangement between an enhancer-rich region of chromosome 8p and the *MYC* locus at 8q24 (Fig. 1C). This event appears to have preceded the *MYC* locus amplification previously documented in this line (12), since high-level amplification at both sides of the breakpoint was evident in alignment data for a control sequencing library (data not shown). The ability of PEAR-ChIP to detect *MYC* rearrangements is of particular interest, given the association of these events with aggressive clinical behavior in multiple tumor types.

PEAR-ChIP identifies known and novel oncogenic rearrangements in diverse B-cell lymphomas

High-grade B-cell lymphomas (HGB), including diffuse large B-cell lymphoma (DLBCL) and related variants such as primary mediastinal large B cell lymphoma (PMBL), show remarkable genetic and epigenetic heterogeneity. We used PEAR-ChIP to profile four HGB cell lines and seven primary HGB biopsies, as well as three lymph node biopsies from patients with chronic lymphocytic leukemia / small lymphocytic lymphoma (CLL/SLL).

To evaluate the efficacy of PEAR-ChIP in detecting known oncogenic rearrangements, we compared the results from our four HGB cell lines to previously published whole genome sequencing data for those same lines (13). WGS detected a total of 6 inter-chromosomal rearrangements or large-scale inversions in these lines associated with a gene known to be recurrently targeted by structural rearrangements in DLBCL according to the Mitelman database. PEAR-ChIP detected all 6 events, including three involving *BCL2*, and three near *MYC* (Supplementary Table S3). Compared to WGS, PEAR-ChIP yielded 2-17 times more supporting reads for those rearrangements, despite a 10-31 fold lower total sequencing depth indicating that PEAR-ChIP can capture such rearrangements with one to two orders of magnitude less sequencing depth. H3K27ac PEAR-ChIP also detected breakpoints at the edges of many amplifications, deletions, and large-scale rearrangements at non-recurrent loci, although these represented only a fraction of the events detected by WGS. Inter-chromosomal rearrangements involving the *IGH* J recombination region showed particularly deep coverage, likely due to strong acetylation extending from the nearby *IGH* μ intronic enhancer, with an average of 34 fragments per 10 million mapped read pairs spanning t(11;14) *IGH-CCND1* rearrangement junctions, and an average of 139 fragments per 10

million mapped read pairs spanning t(14;18) *IGH-BCL2* junctions. Although *BCL6* rearrangements are not represented in our HGB lines, sequencing coverage was high over known breakpoint cluster regions in the *BCL6* locus, with PEAR-ChIP datasets showing an average coverage depth of 69 (standard deviation of 32) fragments per 10 million mapped read-pairs over the 5.3 kb major translocation cluster region in the *BCL6* promoter (14), and an average depth of 130 (standard deviation of 26) fragments per 10 million mapped read-pairs over the 31.2 kb alternate breakpoint region (15), which lies within a highly acetylated "super-enhancer" region upstream of *BCL6* (16,17).

We next focused on large-scale rearrangements involving the *MYC* locus, which were identified by PEAR-ChIP in 4 cell lines (3 HGB and 1 MCL) and one HGB biopsy (Fig. 1C). Notably, all partner loci in these rearrangements showed strong candidate enhancers adjacent to the breakpoint by H3K27ac ChIP-seq signal. Both *IGH* rearrangement breakpoints fell on the 5' side of the *MYC* gene as expected (18), while all non-*IGH* rearrangement breakpoints occurred on the 3' side, with the breakpoint in HGB-05 occurring >400 kb downstream of the *MYC* promoter. One additional *MYC* event, a t(3;8) rearrangement involving the *MYC* and *BCL6* loci in HGB-07, was detected by conventional cytogenetics and FISH, but not by PEAR-ChIP. Deeper sequencing of the HGB-07 control library allowed for localization of rearrangement breakpoints in this case, which occurred in non-acetylated regions, but still linked *MYC* to a strong enhancer as discussed below.

PEAR-ChIP analysis of HGB biopsies detected large-scale rearrangements involving several other known translocation targets, including *BCL2 (n=2), CIITA* (19), and *PDCD1LG2* (20) (Fig 2A, 2B). The *CIITA-IL4R* and *PDCD1LG2-NCOA3* events involve novel translocation partners, with the latter event consisting of an unusual cryptic insertion of the *PDCD1LG2* gene from chromosome 9 into the *NCOA3* gene on chromosome 20. We also detected a t(6;14)(q22;q32) translocation between the *IGHG3* switch region and an intron of *SGK1* (Fig. 2B), likely resulting in *SGK1* inactivation. *SGK1* has not been previously reported as a translocation target, but is located in a region of recurrent genomic deletion, and is a frequent target of inactivating mutations in DLBCL (13). Another novel translocation joined the *IGH* V segment region to a breakpoint 300 kb downstream of the transcriptional regulator *ID2* (Supplementary Fig. S1A-F).

To evaluate the functional significance of PEAR-ChIP-detected rearrangements, we quantified the expression of putative target genes by qRT-PCR across 17 HGB biopsies (Fig. 2C), selected to include at least five cases each of germinal center B-cell (GCB)-DLBCL, activated B-cell (ABC)-DLBCL, and PMBL by immunohistochemistry (IHC), signature gene expression, and clinical criteria (Supplementary Fig. S2A). The anti-apoptotic gene *BCL2* is silenced as part of the normal germinal center gene expression program; as expected, *BCL2* expression was high in the two GCB-DLBCL biopsies with PEAR-ChIP-detected *IGH-BCL2* rearrangements, but low in the other three (Fig. 2C). Similarly, *PDCD1LG2* expression was markedly higher in HGB-01, an ABC-DLBCL that harbors an *NCOA3-PDCD1LG2* rearrangement, than in other DLBCL cases. RT-PCR confirmed expression of an *NCOA3-PDCD1LG2* fusion transcript, as predicted by PEAR-ChIP (Supplementary Fig. S2B). High expression of *PDCD1LG2* is typical of PMBL (21), where it is activated by JAK-STAT signaling and frequent genomic abnormalities (20), but

is unusual in ABC- and GCB-DLBCL. We confirmed low relative expression of *SGK1* and *CIITA* in tumors where PEAR-ChIP detected inactivating rearrangements.

In addition to known rearrangement targets, two other genes showed multiple independent PEAR-ChIP-detected events in our datasets (Supplementary Fig. S1B-C). Events altering the coding sequence of *FOXN3* were seen in both HGB-03 (inter-chromosomal rearrangement) and HGB-04 (deletion of multiple exons). Both HGB-02 and HGB-04 showed deletions involving acetylated elements within the first intron of *MEF2C*, a TF gene that is a mutational target in DLBCL (22). The functional significance of these events is unclear, as MEF2C expression in these cases was similar to that seen in other samples (Supplementary Fig S2C).

PEAR-ChIP identified other small-scale intra-chromosomal deletions and inversions of potential oncogenic significance, including a 120 kb balanced inversion encompassing several exons of *ETV6* (Supplementary Fig. S1D) and a deletion encompassing several exons of *EBF1*. *EBF1* is a frequent mutational target in DLBCL (13), while both *ETV6* (23) and *EBF1* (24) undergo frequent inactivation in immature B-cell neoplasms.

Unlike DLBCL, inter-chromosomal rearrangements are rare in CLL/SLL. PEAR-ChIP analysis of three SLL biopsies did reveal a t(3;7) rearrangement in SLL-03 that disrupted one allele of the *CREB5* gene. In SLL-01, we detected a large interstitial deletion of chromosome 14 that linked the *IGH* μ switch region to the first intron of *ZFP36L1* (Supplementary Fig. S1E), a known recurrent lesion in CLL/SLL (25). We also detected both complete and incomplete (DJ only) immunoglobulin V(D)J rearrangements in all three SLL cases.

Enhancer tandem duplication as a mechanism of oncogene dysregulation in B-cell lymphoma

A particularly interesting class of events detected by PEAR-ChIP consisted of kilobase-scale tandem duplications affecting acetylated candidate enhancers. Such events could represent a mechanism of aberrant oncogene expression. One such duplication in HGB-01 involves a strongly acetylated candidate enhancer region upstream of the rho GTPase-activating gene *TAGAP* (Fig. 2B). qRT-PCR data confirmed that HGB-01 has the highest *TAGAP* expression level of 17 lymphomas evaluated, at 2.4 times the mean expression across samples (Fig. 2C), supporting the enhancer duplication as a gain-of-function event. Genetic polymorphisms within the *TAGAP* locus have been linked to lymphocyte-mediated immune disorders, including rheumatoid arthritis, Crohn disease, and celiac disease, suggesting a role in lymphocyte regulation or proliferation, but, to our knowledge, *TAGAP* has not been previously implicated in lymphoma.

Another notable tandem duplication event was identified upstream of the inducible nitric oxide synthase gene *NOS2* in the PMBL specimen HGB-04 (Supplementary Fig. S1F). The duplicated sequence overlaps a 9 kb region that contains an interferon-responsive enhancer (26). Because interferon-stimulated gene expression is commonly mediated by IRF family TFs, we examined ENCODE ChIP-Seq data from interferon-γ-treated K562 cells, and noted a strong peak of IRF1 binding within the duplicated region. These findings suggest that the

HGB-04 event duplicates a *bona fide* enhancer. *NOS2* expression has been associated with a poor prognosis in classical Hodgkin lymphoma, which shows strong genetic and phenotypic overlaps with PMBL (27). HGB-04 exhibits higher *NOS2* expression than the average across our panel, but is not an outlier in this regard (Supplementary Fig. S2C).

Genomic duplication targets one of several *BCL6*-interacting super-enhancers

PEAR-ChIP analysis of PMBL case HGB-04 identified a 43 kb tandem duplication event encompassing a cluster of acetylated elements upstream of *BCL6* (Fig. 3A), another critical lymphoma oncogene and frequent rearrangement target. To understand whether this region might represent a novel *BCL6* enhancer, we performed a "super-enhancer" analysis (28) on H3K27ac data from our 29 B cell lines and primary samples. This highlighted a known *BCL6*-interacting enhancer region (6,16,17) 150-250 kb upstream of *BCL6* (SE1), which overlaps the alternate breakpoint region, a recurrent site of *BCL6* locus rearrangements (15). It also revealed a second super-enhancer overlapping the HGB-04 duplication at −350 kb (SE2), and a third such region at −500 kb (SE3). All three regions were strongly acetylated in normal centroblasts, GCB-DLBCL tumor biopsies, and most HGB cell lines, but lacked acetylation in non-germinal center B cells, MCL and SLL. The few HGB samples that lacked *BCL6* super-enhancer activation included cases with evidence for a non-germinal center oncogenic program, such as our ABC-DLBCL sample HGB-01 and Oci-Ly-3, a well-characterized ABC-DLBCL cell line. We used chromosome conformation capture (3C) analysis of GCB-DLBCL lymphoma cell lines (Supplementary Fig. S3A) to confirm looping of elements from super-enhancer regions to the *BCL6* promoter, consistent with roles in activating this oncogene. Intriguingly, our PMBL case, HGB-04, showed a distinct acetylation pattern across these regions, with only the duplicated enhancer region, SE2, showing strong acetylation. Despite lacking acetylation at most of the *BCL6* enhancers seen in GCB-DLBCL, HGB-04 showed stronger *BCL6* expression than 3 of 6 GCB-DLBCL cases, and all 5 ABC-DLBCL cases evaluated (Fig. 3B), suggesting that the tandem duplication of SE2 may drive *BCL6* expression in this case.

Coordinated acetylation of BCL6 enhancers is driven by MEF2B binding and p300 recruitment

To better understand the basis for coordinated activation of *BCL6* enhancers, we used ChIP-Seq in HGB cell lines to map MEF2B, a germinal center-specific TF known to drive *BCL6* expression (29). We did not detect substantial MEF2B binding in the vicinity of the *BCL6* promoter. Rather, we observed strong, focal MEF2B binding at acetylated elements within *BCL6* super-enhancer regions, including four sites in SE1, one in SE2, and two in SE3 (Fig. 3C). These patterns were reproducible by two distinct MEF2B antibodies, and in five cell lines (Supplementary Fig. S3B-C). Since other MEF2 family proteins activate gene expression through recruitment of the p300 acetyltransferase to distal enhancers, we performed ChIP-Seq for p300. We observed a high degree of correlation between MEF2B and p300 binding at distal sites across the *BCL6* locus (Fig. 3C), and genome-wide (Supplementary Fig. S4A). In contrast, p300 binding showed little correspondence to the distribution of three other B-cell TFs that we mapped (PU.1, Pax5, and Bach2). Genome-wide *de novo* motif analysis of all MEF2B ChIP-Seq datasets revealed a top-ranked motif similar to that published for other MEF2 family factors, and a MEF2-like motif represented

the fourth most significantly enriched motif in p300 ChIP-seq peaks (Supplementary Fig. S4B-C). Intriguingly, sites within SE1 that were bound by other TFs, but not by MEF2B, showed minimal p300 binding, and retained acetylation in non-germinal center phenotype populations (Fig. 3A and 3C).

To test whether MEF2B expression was sufficient to drive *BCL6* enhancer acetylation, we used an inducible lentiviral vector to express HA-tagged MEF2B in two MCL cell lines, which show low basal expression of *BCL6* transcripts (Fig. 3D) and MEF2B protein (Supplementary Fig. S3C), as well as two HGB lines. Induction of MEF2B expression resulted in an increase in *BCL6* expression in all cell lines, although the relative increase was greater in MCL lines (Fig. 3D). ChIP-Seq analysis in the Jeko-1 MCL line revealed a specific increase in H3K27ac at MEF2B binding sites in MEF2B transgene-expressing cells, but not at intervening elements within the *BCL6* super-enhancers (Fig. 3E). These data support a direct role for MEF2B in the activation of enhancers that drive *BCL6* expression in human lymphomas.

Native *MYC* locus enhancers show lymphoma subtype-specific activity

The *MYC* gene lies within a nearly 4-megabase locus devoid of other spliced protein-coding genes. This locus contains multiple enhancers that drive *MYC* expression in specific lineages and cancer types, including an immature T cell-specific enhancer (30) and a myeloid cell-specific enhancer (3), which reside 1.4 and 1.8 Mb downstream of *MYC*, respectively. Tissue-specific candidate *MYC* enhancers have also been identified for breast, colon, and prostate carcinomas (31). Although *MYC* enhancers from other cancers showed little acetylation in our B-cell lymphoma datasets, distinct patterns of acetylation identified other enhancer-like elements in the *MYC* locus (Fig 4A-C). Elements located between 235-535 kb downstream of *MYC* were frequently acetylated in HGB biopsies and cell lines (Fig. 4A,C), as well as in normal germinal center B cells (centroblasts). Elements in this region are syntenic to enhancers that interact with RNA polymerase II at the *MYC* promoter in mouse activated B cells (6,32), suggesting that they may represent human *MYC* enhancers. We used 3C in HGB cell lines to demonstrate that the *MYC* promoter physically interacts with candidate enhancers in this region (hereafter “3’ *MYC*-interacting region”), but not with the myeloid or T cell enhancers (Fig. 4A and data not shown). Intriguingly, the 3’ *MYC*-interacting region is targeted by recurrent focal somatic amplifications in plasma cell myeloma (33), further supporting a significant oncogenic role for this region in B-cell malignancies.

Although candidate enhancers in the 3’ *MYC*-interacting region were strongly acetylated in most HGB samples, they lacked acetylation in HGB biopsies and cell lines with genomic rearrangement of the *MYC* locus (Fig. 4C). Absence of acetylation in these cases appears to be biallelic, and independent of the position of the *MYC* locus breakpoint. If enhancers in this region are responsible for driving *MYC* expression, they would presumably be dispensable in the setting of translocations that bring strong heterologous enhancers into proximity with *MYC*. Their lack of acetylation in *MYC*-rearranged tumors could reflect negative-feedback mechanisms that suppress acetylation in the setting of high MYC expression. In support of this hypothesis, lentiviral overexpression of *MYC* in a non-

rearranged HGB cell line caused a significant reduction in candidate enhancer acetylation within the 3' *MYC*-interacting region (Supplementary Fig. 5A-B).

In contrast to HGB samples, most elements in the 3' *MYC*-interacting region lacked acetylation in our MCL and SLL datasets, and in non-germinal center B cells from peripheral blood (PBL) (Fig. 4B-C). Instead, these populations showed specific acetylation of a cluster of candidate enhancers 400-600 kb upstream of *MYC* (hereafter "5' *MYC*-interacting region") that interact with the *MYC* promoter by 3C in MCL and SLL biopsies. Notably, the 5' *MYC*-interacting region corresponds to a site of recurrent amplification in CLL/SLL (34), and contains regulatory elements that have previously been shown to interact with the *MYC* promoter and activate *MYC* transcription in *in vitro*-transformed B-lymphoblastoid cell lines via binding of the Epstein-Barr virus oncoprotein EBNA2 (35), demonstrating that elements within this region can function as *bona fide MYC* enhancers.

Polymorphisms linked to hereditary risk for specific lymphomas are associated with *MYC* locus enhancers that show subtype-specific acetylation

Genome-wide association studies (GWAS) have identified single-nucleotide polymorphisms (SNPs) in a small number of loci that correlate with altered hereditary risk for specific lymphoma types. Remarkably, we note that the 3' *MYC*-interacting region, which shows centroblast and DLBCL/PMBL-specific enhancer acetylation, contains polymorphisms linked to hereditary risk for DLBCL (one of 4 known loci genome-wide)(36) and Hodgkin lymphoma (one of 6 known loci genome-wide)(37). Furthermore, the 5' *MYC*-interacting region, which shows SLL and MCL-specific enhancer acetylation, contains a polymorphism linked to hereditary risk for CLL/SLL (one of 22 known loci genome-wide) (38). Intergenic polymorphisms predicted as causal for disease risk are frequently located within the central TF binding region of enhancers, often adjacent to or directly altering TF binding motifs (39,40), suggesting that a similar mechanism may occur in lymphoma. Indeed, for each lymphoma type, we could identify at least one lead or strongly linked SNP ($r^2 > 0.9$) in the *MYC* locus that coincides precisely with a DNase hypersensitive site in an enhancer with subtype-specific acetylation (Supplementary Fig S5C-E). Further analysis revealed that the implicated SNPs alter or are adjacent to a high-confidence motif for a lymphoid TF. We note that rs7826019, one of the two enhancer-associated Hodgkin lymphoma SNPs that we highlighted, has been previously suggested as a likely functional SNP for this GWAS locus (41). The surrounding enhancer is acetylated in several HGB cases, including a biopsy of PBML, a disease that shares many common biological features with Hodgkin lymphoma (21). Taken together, our findings suggest that alternate regulatory elements located hundreds of kilobases upstream and downstream of the *MYC* gene are acetylated at distinct B cell developmental stages, and play oncogenic roles in specific lymphoma types.

A t(3;8) translocation is characterized by *MYC* recruitment of *BCL6* enhancers

Identification of candidate enhancers in the *BCL6* and *MYC* loci allowed us investigate aberrant enhancer-promoter relationships in the setting of the t(3;8)(q27;q24) rearrangement that directly links the *MYC* and *BCL6* loci in the GCB-DLBCL sample HGB-07. HGB-07 showed the highest *MYC* expression by qRT-PCR of any of our lymphoma samples (Fig. 2C), but *BCL6* expression in HGB-07 was the lowest of any GCB-DLBCL sample, although

higher than in all ABC-DLBCL samples (Fig. 3B), suggesting that *MYC*, but not *BCL6*, was activated by this rearrangement. Interestingly, the *BCL6* and *MYC* locus breakpoints in HGB-07 occur directly between each gene and its native enhancer regions, resulting in an "enhancer swap" (Fig. 5A-B). The 3' *MYC*-interacting region in HGB-07 lacked acetylation, similar to the findings in lymphomas with known heterologous activating rearrangements of *MYC*. In contrast, the *BCL6* super-enhancers in HGB-07 case were broadly acetylated, suggesting that these could function to activate *MYC* on the rearranged allele. This hypothesis was supported by comparison of 3C data from HGB-07 to data from HGB-06, a lymphoma that lacked a *MYC* rearrangement, but showed strong *BCL6* and moderate *MYC* expression by qRT-PCR and IHC. In both cases, we detected the expected interactions between the *BCL6* and *MYC* promoters and candidate enhancers in their native locus (Fig. 5C-D). We then used the same enhancer primers to measure interactions with the opposite gene promoter. We detected strong interactions between the *MYC* promoter and elements within the *BCL6* SE1 and SE2 regions in HGB-07, but no such interactions in the non-rearranged tumor, HGB-06. In contrast, we did not see significant interaction between the 3' *MYC*-interacting region and the *BCL6* promoter in either case. Our findings strongly suggest that the oncogenic effect of this t(3;8) rearrangement is heterologous activation of *MYC* by *BCL6* locus enhancers (see model in Fig. 5E).

Discussion

We have leveraged chromatin profiling and a novel analytic approach to identify genomic rearrangements associated with active enhancers, revealing both known "enhancer hijacking" events as well as novel enhancer duplications of likely oncogenic significance in lymphoma. Our focused investigation of two recurrently altered loci, *MYC* and *BCL6*, in the presence and absence of rearrangements and across multiple lymphoma subtypes, provided novel insights regarding the role of native and rearranged enhancers in controlling these critical oncogenes. Understanding such mechanisms may be of particular clinical significance, given the ongoing development of drugs that target enhancer function (42). Moreover, we believe that the efficient PEAR-ChIP approach described here expands future possibilities for identification of enhancer-associated rearrangements in research or clinical settings.

PEAR-ChIP efficiently detected genomic rearrangements in lymphoma samples, despite the fact that our datasets cover only a small fraction of the genome at high sequencing depth. Since many oncogene rearrangements drive lymphoma by juxtaposing powerful enhancers with target oncogenes, it is not surprising that many such events should occur sufficiently close to strong enhancers to allow for breakpoint detection after enrichment for acetylated chromatin. Additionally, recent studies have demonstrated that AID, an important driver of DNA damage and genomic rearrangements in lymphomagenesis, is specifically targeted to strongly acetylated regions of the genome, which include both the immunoglobulin switch regions and a subset of strongly active enhancers genome-wide (6,7). By providing deep coverage of acetylated regions, PEAR-ChIP therefore focuses specifically on regions of the genome likely to harbor aberrant AID-induced rearrangements. Further studies are needed to determine the value of PEAR-ChIP analysis in cancer types other than lymphoma. One potentially fruitful strategy could be to complement the enhancer activation profiling and

focused high-resolution breakpoint detection of PEAR-ChIP with a low-resolution, genome-wide approach such as long-insert mate-pair sequencing for efficient genome-wide correlation of enhancer activity and genomic rearrangements.

Our findings also provide novel insight regarding the activity of lymphoma subtype-specific candidate enhancers in the native loci of the oncogenes *MYC* and *BCL6*. Such native locus enhancers may drive oncogene expression in lymphomas without rearrangements, and may be further activated by focal duplication or amplification events. Additionally, our analysis suggests that germline polymorphisms in the *MYC* locus linked to altered risk for specific lymphoma types may directly affect enhancers that are selectively active in the corresponding lymphomas. Additional work is needed to demonstrate whether the specific enhancer-associated SNPs highlighted here are truly causal for altered lymphoma risk, the mechanisms by which they act, and the implications for lymphoma prevention and treatment. Importantly, we found that a master TF for *BCL6* expression, MEF2B, drives acetylation of specific individual elements within multiple 'super-enhancers' that converge on the *BCL6* promoter. Understanding cross-talk and synergy between individual TF units in this array could be an important area for future study, and lies at the crux of more general questions regarding the super-enhancer concept (43).

Finally, our investigation sheds light on the function of a t(3;8) *BCL6-MYC* rearrangement, a recurrent event in B-cell lymphomas (44). Among DLBCL cases, *BCL6* rearrangements are most often seen in ABC-DLBCL (45), and often involve partner loci with strong activating elements, such as *IGH*, *IGK*, and *IGL*, which are thought to activate expression of *BCL6* in the absence of an intact germinal center program. In contrast, our data shows that the t(3;8) event in HGB-07, a case of GCB-DLBCL, is unlikely to be a *BCL6* activating event, but rather results in *BCL6* enhancers interacting with, and likely activating, *MYC*. Thus, the *BCL6* locus may serve as either the recipient or the donor of activating regulatory elements in distinct rearrangements. To our knowledge, this is the first example of any oncogene locus capable of playing such a dual role. This finding has important implications for defining a group of aggressive B-cell lymphomas bearing simultaneous activating translocations of *MYC* plus one or both of the oncogenes *BCL2* and *BCL6*, referred to as "double hit lymphomas" (DHL) or "triple hit lymphomas" (THL) (46). These cases have been associated with a poor prognosis, and are frequently treated with an intensified initial chemotherapeutic regimen. In some series, the presence of a t(3;8) *BCL6-MYC* rearrangement, or positive results on break-apart FISH-studies for both the *BCL6* and *MYC* loci (without identifying partner loci) have been considered sufficient to classify a case as DHL. Our data challenges this assumption by demonstrating that the t(3;8) rearrangement in HGB-07 is unlikely to be a *BCL6*-activating event, but rather represents *MYC* activation by *BCL6* locus enhancers, similar to other "single-hit" *MYC*-activating rearrangements. We would suggest that lymphomas bearing t(3;8) *BCL6-MYC* rearrangements should be distinguished from cases with separate activating translocations of *BCL6* and *MYC* to different partner loci, and propose the term "pseudo double-hit rearrangement" for events of the type seen in HGB-07. More generally, given the structural and functional diversity of *BCL6* locus rearrangements, we would caution against the assumption that all FISH-detected

BCL6 rearrangements carry biologically similar implications for the purposes of research or clinical diagnostic practice.

Materials and Methods

Cell lines and lymphoma samples

Lymphoma cell lines were generous gifts from Dr. Mark Minden at the Ontario Cancer Institute (Oci-Ly-1 and Oci-Ly-7, acquired in 2010), were purchased from ATCC (Pfeiffer and Toledo, acquired in 2013) or were obtained from the Broad-Novartis Cancer Cell Line Encyclopedia (all others, acquired between 2012 and 2014) and were grown in IMDM + 20% FCS (Oci-Ly-1 and Oci-Ly-7) or RPMI + 10-20% FCS (all others). Pfeiffer and Toledo were validated at ATCC by short tandem repeat profiling, while identity of all other lines was validated by Sanger sequencing of unique polymorphisms at the time of acquisition and frozen stock generation in our laboratory. With the exception of lentivirus experiments, all lines were grown for <10 passages in our laboratory between validation sequencing and crosslinking for ChIP-Seq. ChIP-Seq profiling of normal B cell populations was described previously (40). Frozen excess surgical tissue from human lymphomas was obtained from the Massachusetts General Hospital Pathology Service under DF/HCC protocol 13-594. Informed consent was obtained from each subject. Frozen sections and paraffin IHC were reviewed, and blocks with >80% lymphoma cells were used. IHC for CD10, BCL6, IRF4, and MYC were performed on paraffin sections of lymphoma biopsies according to protocols validated for clinical diagnostic use by the MGH Pathology Service, and DLBCL cases were preliminarily classified as GCB- or non-GCB-DLBCL by the Hans algorithm (47). Interphase FISH analysis for *MYC* rearrangement was performed with the Vysis LSI *MYC* Dual Color, Break Apart Rearrangement Probe (Abbott Molecular).

ChIP-Seq

For histone modification and TF ChIP-Seq in cell lines, 10-20 million cells were crosslinked in growth media + 1% formaldehyde for 10 min. at 37°C, quenched for 5 min. with 125 mM glycine, washed twice in cold PBS with protease inhibitors, and stored at −80°C. For primary lymphoma samples, tumor cellularity from the frozen block was confirmed by H&E frozen section by a board-certified hematopathologist (RR), and the block was trimmed as needed. 25 micron sections were then cut to a total of ~50 mg of tissue for each ChIP-Seq chromatin prep. Frozen sections were resuspended and dissociated in PBS + PI + 10 mM sodium butyrate, formaldehyde was added to 1%, and crosslinking, quenching and washing were performed as above. Chromatin immunoprecipitation and sequencing library preparation were performed by standard methods, with details provided in the Supplementary Methods.

Paired-end sequencing of H3K27ac ChIP and an un-enriched chromatin control library was performed on a HiSeq 2500 or NextSeq for all primary lymphoma samples and for 8 cell lines, with read lengths of 36 bp + 25 bp or 38 bp + 38 bp. Based on analysis of mapped read-pairs, paired-end libraries contained an average fragment size of 303 bp (range 252-332 bp) with 95% of fragments at least 147-225 bp and at most 398-498 bp in length. Single-end sequencing was used for other samples. Single- and paired-end reads were aligned to hg19

using BWA-ALN and filtered to remove PCR duplicates and reads mapping to >2 sites genome-wide. ChIP-Seq tracks were generated with 'igvtools count' and visualized with IGV. Super-enhancer analysis of H3K27ac ChIP-Seq was performed with MACS and ROSE as described (28). TF and p300 ChIP-seq peak calling were performed with HOMER, using the "factor" style. *De novo* motif analysis of TF and p300 peaks was performed using HOMER. ChIP datasets are available through Gene Expression Omnibus accession GSE69558, and dbGaP accession phs000939.v1.p1.

PEAR-ChIP Rearrangement detection

dRanger and BreakPointer (10) were used to identify rearrangements in paired-end H3K27ac alignment files. Customized filtering criteria are detailed in the Supplementary Methods.

RT-PCR, qRT-PCR and ChIP-PCR

25 micron sections of frozen tumor tissue were used for RNA extraction via sequential Trizol and column purification with DNase digestion, followed by reverse transcription. RT-PCR primers for confirmation of the *NCOA3-PDCD1LG2* fusion transcript consisted of a forward primer within *NCOA3* exon 1, and a reverse primer located after the first splice junction of *PDCD1LG2*. To support our classification of biological subtype for high-grade lymphomas, we designed qPCR primers for signature genes identified as significantly up-regulated in PMBL versus DLBCL in two expression microarray studies (21,48) and for selected GCB-DLBCL and ABC-DLBCL signature genes, as well as all five housekeeping genes, from a validated assay for lymphoma expression classification (49). Syber Green qRT-PCR was used to measure the expression of rearrangement target genes, signature genes, and housekeeping genes, with *RPLPO* used as a reference gene on all plates. Relative quantity and 95% confidence intervals were calculated for each gene by the delta-delta Ct method and ABI 7500 software. All relative expression values for each sample were then divided by a normalization factor, calculated as the geometric mean of the quantities of each of the five housekeeping genes in that sample relative to sample HGB-01. For cell line experiments, SYBER Green qRT-PCR was used to measure *BCL6* expression by the relative standard curve method with normalization to *RPLP0*. The relative change in *MYC* locus promoter and enhancer acetylation were quantified by SYBER green qPCR of ChIP DNA, with normalization to input chromatin and primers recognizing control enhancers adjacent to the *CD79A* and *PTPRC* (CD45) genes. All primer sequences are available on request.

Single nucleotide polymorphism linkage and motif analysis

MYC locus polymorphisms linked to germline risk for development of DLBCL, Hodgkin lymphoma, and chronic lymphocytic leukemia were obtained from meta-analyses of genome-wide association studies (GWAS) conducted in populations of British, European-American, and other Western European origin (36–38). We used the 1000 Genomes Project Browser to identify all SNPs in strong linkage disequilibrium ($r^2 > 0.8$) to identified GWAS index SNPs in both the GBR and CEU population subgroups. Index SNPs and all linked SNPs were queried for overlap with ENCODE uniform DNase hypersensitivity (DNAse HS) peaks for 10 B-lymphoblastoid cell lines and 2 other B cell populations. HOMER findMotifs

was used to identify and score known TF binding motifs in the presence of the reference or variant allele for each SNP in a DNase HS site.

Chromosome conformation capture

3C was performed on 10 million cultured cells or 20-40 mg of 25 micron-sectioned frozen tissue according to published protocols (50). Taqman probe and primer sets for the *BCL6* locus were adapted from previous reports (16). Probe and primer sets for EcoRI 3C at the *MYC* locus were designed with Primer3 for mutual compatibility with *BCL6* 3C primers. All comparisons reflected equal input DNA quantity as determined by SYBER green qPCR. Taqman qPCR was performed in 2-3 replicates for all sites, and a Ct value of 40 was assigned for all reactions with Ct ≥ 40. Values are expressed as relative quantity $[2^{-(\text{Cttest} - \text{Ctprom})}]$ in comparison to control primers spanning the EcoRI site at the *MYC* promoter, and error bars reflect the standard error of the mean for replicates. HindIII-based 3C was performed to evaluate the T-cell-specific *MYC* enhancer with published probes and primers (30). Probe and primer sequences are available on request.

Lentiviral constructs

An open reading frame encoding *MEF2B* (CCDS 46024.1) with a c-terminal HA tag was cloned into pINDUCER-20, and *MYC* (CCDS 6359.2, amino acids 16-454) was cloned into pLX-304. Lentivirus was produced in HEK-293T cells and subject to 0.45-μm filtration. Cell lines were transduced with lentiviral supernatants by spinfection for 90 minutes in the presence of polybrene. After 48 hour recovery, transduced cells were selected by blastocidin (5 days, pLX-304), or G418 (10+ days, pINDUCER-20). pINDUCER-20 expression was induced with 100 ng/mL doxycycline 48 hours prior to cell harvest.

Western Blot

Western blots were performed by standard protocols with the following antibodies: MEF2B (ab33540, Abcam and HPA004734, Atlas), MEF2C (D80C1, Cell Signalling), and TBP (1TBP18, Abcam)

Supplementary Material

Refer to Web version on PubMed Central for supplementary material.

Acknowledgments

The authors would like to thank all clinicians and staff who facilitated identification and consenting of patients, including J. Abramson, R. Takvorian, J. Barnes, Y. Chen, T. Spitzer, B. McGree, A. Crawford, J. Ramirez, N. Birrer, and H. Martinson, as well as C. Desilus for technical assistance with FISH assays. We thank Nancy L. Harris for thoughtful feedback on the manuscript. R. Ryan, A. Sohani, and E. Hochberg gratefully acknowledge funding support from an anonymous foundation.

Russell Ryan received funding from NIH training grants T32GM007748 and T32CA009216.

Bradley Bernstein received funding from ENCODE, the Leukemia and Lymphoma Society, and the Howard Hughes Medical Institute.

References

1. Duan H, Xiang H, Ma L, Boxer LM. Functional long-range interactions of the IgH 3' enhancers with the bcl-2 promoter region in t(14;18) lymphoma cells. Oncogene. 2008; 27:6720–8. [PubMed: 18695675]
2. Northcott P, Lee C, Zichner T, Stütz AM, Erkek S, Kawauchi D, et al. Enhancer hijacking activates GFI1 family oncogenes in medulloblastoma. Nature. 2014; 511:428–34. [PubMed: 25043047]
3. Shi J, Whyte W, Zepeda-Mendoza CJ, Milazzo JP, Shen C, Roe J-S, et al. Role of SWI/SNF in acute leukemia maintenance and enhancer-mediated Myc regulation. Genes Dev. 2013; 27:2648–62. [PubMed: 24285714]
4. Creyghton MP, Cheng AW, Welstead GG, Kooistra T, Carey BW, Steine EJ, et al. Histone H3K27ac separates active from poised enhancers and predicts developmental state. Proc Natl Acad Sci U S A. 2010; 107:21931–6. [PubMed: 21106759]
5. Ernst J, Kheradpour P, Mikkelsen TS, Shoresh N, Ward LD, Epstein CB, et al. Mapping and analysis of chromatin state dynamics in nine human cell types. Nature. 2011; 473:43–9. [PubMed: 21441907]
6. Qian J, Wang Q, Dose M, Pruett N, Kieffer-Kwon K-R, Resch W, et al. B cell super-enhancers and regulatory clusters recruit AID tumorigenic activity. Cell. 2014; 159:1524–37. [PubMed: 25483777]
7. Meng F, Du Z, Federation A, Hu J, Wang Q, Kieffer-Kwon K-R, et al. Convergent transcription at intragenic super-enhancers targets AID-initiated genomic instability. Cell. 2014; 159:1538–48. [PubMed: 25483776]
8. Swerdlow, SH.; Campo, E.; Harris, NL.; Jaffe, ES.; Pileri, SA.; Stein, H., et al., editors. WHO Classification of Tumors of Haematopoietic and Lymphoid Tissues. 4th. International Agency for Research on Cancer; Lyon: 2008.
9. Wiestner A, Tehrani M, Chiorazzi M, Wright G, Gibellini F, Nakayama K, et al. Point mutations and genomic deletions in CCND1 create stable truncated cyclin D1 mRNAs that are associated with increased proliferation rate and shorter survival. Blood. 2007; 109:4599–606. [PubMed: 17299095]
10. Drier Y, Lawrence MS, Carter SL, Stewart C, Gabriel SB, Lander ES, et al. Somatic rearrangements across cancer reveal classes of samples with distinct patterns of DNA breakage and rearrangement-induced hypermutability. Genome Res. 2013; 23:228–35. [PubMed: 23124520]
11. Kluk MJ, Ashworth T, Wang H, Knoechel B, Mason EF, Morgan EA, et al. Gauging NOTCH1 Activation in Cancer Using Immunohistochemistry. PLoS One. 2013; 8:e67306. [PubMed: 23825651]
12. Camps J, Salaverria I, Garcia MJ, Prat E, Beà S, Pole JC, et al. Genomic imbalances and patterns of karyotypic variability in mantle-cell lymphoma cell lines. Leuk Res. 2006; 30:923–34. [PubMed: 16448697]
13. Morin RD, Mungall K, Pleasance E, Mungall AJ, Goya R, Huff RD, et al. Mutational and structural analysis of diffuse large B-cell lymphoma using whole-genome sequencing. Blood. 2013; 122:1256–65. [PubMed: 23699601]
14. Bastard C, Deweindt C, Kerckaert JP, Lenormand B, Rossi A, Pezzella F, et al. LAZ3 rearrangements in non-Hodgkin's lymphoma: correlation with histology, immunophenotype, karyotype, and clinical outcome in 217 patients. Blood. 1994; 83:2423–7. [PubMed: 8167331]
15. Butler MP, Iida S, Capello D, Rossi D, Rao PH, Nallasivam P, et al. Alternative translocation breakpoint cluster region 5′ to BCL-6 in B-cell non-Hodgkin's lymphoma. Cancer Res. 2002; 62:4089–94. [PubMed: 12124346]
16. Ramachandrareddy H, Bouska A, Shen Y, Ji M, Rizzino A, Chan WC, et al. BCL6 promoter interacts with far upstream sequences with greatly enhanced activating histone modifications in germinal center B cells. Proc Natl Acad Sci U S A. 2010; 107:11930–5. [PubMed: 20547840]
17. Chapuy B, McKeown MR, Lin CY, Monti S, Roemer MGM, Qi J, et al. Discovery and Characterization of Super-Enhancer-Associated Dependencies in Diffuse Large B Cell Lymphoma. Cancer Cell. 2013; 24:777–90. [PubMed: 24332044]
18. Gostissa M, Yan CT, Bianco JM, Cogné M, Pinaud E, Alt FW. Long-range oncogenic activation of Igh-c-myc translocations by the Igh 3' regulatory region. Nature. 2009; 462:803–7. [PubMed: 20010689]

19. Steidl C, Shah SP, Woolcock BW, Rui L, Kawahara M, Farinha P, et al. MHC class II transactivator CIITA is a recurrent gene fusion partner in lymphoid cancers. Nature. 2011; 471:377–81. [PubMed: 21368758]
20. Twa DDW, Chan FC, Ben-Neriah S, Woolcock BW, Mottok A, Tan KL, et al. Genomic rearrangements involving programmed death ligands are recurrent in primary mediastinal large B-cell lymphoma. Blood. 2014; 123:2062–5. [PubMed: 24497532]
21. Rosenwald A, Wright G, Leroy K, Yu X, Gaulard P, Gascoyne RD, et al. Molecular diagnosis of primary mediastinal B cell lymphoma identifies a clinically favorable subgroup of diffuse large B cell lymphoma related to Hodgkin lymphoma. J Exp Med. 2003; 198:851–62. [PubMed: 12975453]
22. Lohr JG, Stojanov P, Lawrence MS, Auclair D, Chapuy B, Sougnez C, et al. Discovery and prioritization of somatic mutations in diffuse large B-cell lymphoma (DLBCL) by whole-exome sequencing. Proc Natl Acad Sci U S A. 2012; 109:3879–84. [PubMed: 22343534]
23. O'Connor HE, Butler T a, Clark R, Swanton S, Harrison CJ, Secker-Walker LM, et al. Abnormalities of the ETV6 gene occur in the majority of patients with aberrations of the short arm of chromosome 12: a combined PCR and Southern blotting analysis. Leukemia. 1998; 12:1099–106. [PubMed: 9665196]
24. Mullighan CG, Goorha S, Radtke I, Miller CB, Coustan-Smith E, Dalton JD, et al. Genome-wide analysis of genetic alterations in acute lymphoblastic leukaemia. Nature. 2007; 446:758–64. [PubMed: 17344859]
25. Pospisilova H, Baens M, Michaux L, Stul M, Van Hummelen P, Van Loo P, et al. Interstitial del(14)(q) involving IGH: a novel recurrent aberration in B-NHL. Leukemia. 2007; 21:2079–83. [PubMed: 17525729]
26. De Vera ME, Shapiro R a, Nussler a K, Mudgett JS, Simmons RL, Morris SM, et al. Transcriptional regulation of human inducible nitric oxide synthase (NOS2) gene by cytokines: initial analysis of the human NOS2 promoter. Proc Natl Acad Sci U S A. 1996; 93:1054–9. [PubMed: 8577713]
27. Campos AHJFM, Aldred VL, Ribeiro KCB, Vassallo J, Soares FA. Role of immunoexpression of nitric oxide synthases by Hodgkin and Reed-Sternberg cells on apoptosis deregulation and on clinical outcome of classical Hodgkin lymphoma. Mol Cell Biochem. 2009; 321:95–102. [PubMed: 18830569]
28. Hnisz D, Abraham BJ, Lee TI, Lau A, Saint-André V, Sigova A a, et al. Super-enhancers in the control of cell identity and disease. Cell. 2013; 155:934–47. [PubMed: 24119843]
29. Ying CY, Dominguez-Sola D, Fabi M, Lorenz IC, Hussein S, Bansal M, et al. MEF2B mutations lead to deregulated expression of the oncogene BCL6 in diffuse large B cell lymphoma. Nat Immunol. 2013; 14:1084–92. [PubMed: 23974956]
30. Herranz D, Ambesi-Impiombato A, Palomero T, Schnell S, Belver L, Wendorff A, et al. A NOTCH1-driven MYC enhancer promotes T cell development, transformation and acute lymphoblastic leukemia. Nat Med. 2014; 20:1130–7. [PubMed: 25194570]
31. Ahmadiyeh N, Pomerantz MM, Grisanzio C, Herman P, Jia L, Almendro V, et al. 8q24 prostate, breast, and colon cancer risk loci show tissue-specific long-range interaction with MYC. Proc Natl Acad Sci U S A. 2010; 107:9742–6. [PubMed: 20453196]
32. Kieffer-Kwon K-R, Tang Z, Mathe E, Qian J, Sung M-H, Li G, et al. Interactome Maps of Mouse Gene Regulatory Domains Reveal Basic Principles of Transcriptional Regulation. Cell. 2013; 155:1507–20. [PubMed: 24360274]
33. Affer M, Chesi M, Chen WD, Keats JJ, Demchenko YN, Tamizhmani K, et al. Promiscuous MYC locus rearrangements hijack enhancers but mostly super-enhancers to dysregulate MYC expression in multiple myeloma. Leukemia. 2014; 28:1725–35. [PubMed: 24518206]
34. Edelmann J, Holzmann K, Miller F, Winkler D, Bühler A, Zenz T, et al. High-resolution genomic profiling of chronic lymphocytic leukemia reveals new recurrent genomic alterations. Blood. 2012:4783–94. [PubMed: 23047824]
35. Zhao B, Zou J, Wang H, Johannsen E, Peng C -w. Quackenbush J, et al. Epstein-Barr virus exploits intrinsic B-lymphocyte transcription programs to achieve immortal cell growth. Proc Natl Acad Sci. 2011; 108:14902–7. [PubMed: 21746931]

36. Cerhan JR, Berndt SI, Vijai J, Ghesquières H, McKay J, Wang SS, et al. Genome-wide association study identifies multiple susceptibility loci for diffuse large B cell lymphoma. Nat Genet. 2014; 46:1233–8. [PubMed: 25261932]
37. Cozen W, Timofeeva MN, Li D, Diepstra a, Hazelett D, Delahaye-Sourdeix M, et al. A meta-analysis of Hodgkin lymphoma reveals 19p13.3 TCF3 as a novel susceptibility locus. Nat Commun. 2014; 5:3856. [PubMed: 24920014]
38. Berndt SI, Skibola CF, Joseph V, Camp NJ, Nieters A, Wang Z, et al. Genome-wide association study identifies multiple risk loci for chronic lymphocytic leukemia. Nat Genet. 2013; 45:868–76. [PubMed: 23770605]
39. Maurano MT, Humbert R, Rynes E, Thurman RE, Haugen E, Wang H, et al. Systematic Localization of Common Disease-Associated Variation in Regulatory DNA. Science (80−). 2012; 337:1190–5.
40. Farh KK, Marson A, Zhu J, Kleinewietfeld M, Housley WJ, Beik S, et al. Genetic and epigenetic fine mapping of causal autoimmune disease variants. Nature. 2015; 518:337–43. [PubMed: 25363779]
41. Schaub MA, Boyle AP, Kundaje A, Frazer KA. Linking disease associations with regulatory information in the human genome. Genome Res. 2012; 22:1748–59. [PubMed: 22955986]
42. Lovén J, Hoke H, Lin C, Lau A, Bradner J, Lee T, et al. Selective inhibition of tumor oncogenes by disruption of super-enhancers. Cell. 2013; 153:320–34. [PubMed: 23582323]
43. Pott S, Lieb JD. What are super-enhancers? Nat Genet. 2014; 47:8–12. [PubMed: 25547603]
44. Pillai RK, Sathanoori M, Van Oss SB, Swerdlow SH. Double-hit B-cell Lymphomas With BCL6 and MYC Translocations Are Aggressive, Frequently Extranodal Lymphomas Distinct From BCL2 Double-hit B-cell Lymphomas. Am J Surg Pathol. 2013; 37:323–32. [PubMed: 23348205]
45. Iqbal J, Greiner TC, Patel K, Dave BJ, Smith L, Ji J, et al. Distinctive patterns of BCL6 molecular alterations and their functional consequences in different subgroups of diffuse large B-cell lymphoma. Leukemia. 2007; 21:2332–43. [PubMed: 17625604]
46. Aukema SM, Siebert R, Schuuring E, van Imhoff GW, Kluin-Nelemans HC, Boerma E-J, et al. Double-hit B-cell lymphomas. Blood. 2011; 117:2319–31. [PubMed: 21119107]
47. Hans CP, Weisenburger DD, Greiner TC, Gascoyne RD, Delabie J, Ott G, et al. Confirmation of the molecular classification of diffuse large B-cell lymphoma by immunohistochemistry using a tissue microarray. Blood. 2004; 103:275–82. [PubMed: 14504078]
48. Savage KJ, Monti S, Kutok JL, Cattoretti G, Neuberg D, De Leval L, et al. The molecular signature of mediastinal large B-cell lymphoma differs from that of other diffuse large B-cell lymphomas and shares features with classical Hodgkin lymphoma. Blood. 2003; 102:3871–9. [PubMed: 12933571]
49. Scott DW, Wright GW, Williams PM, Lih C-J, Walsh W, Jaffe ES, et al. Determining cell-of-origin subtypes of diffuse large B-cell lymphoma using gene expression in formalin-fixed paraffin embedded tissue. Blood. 2014:1214–7. [PubMed: 24398326]
50. Hagège H, Klous P, Braem C, Splinter E, Dekker J, Cathala G, et al. Quantitative analysis of chromosome conformation capture assays (3C-qPCR). Nat Protoc. 2007; 2:1722–33. [PubMed: 17641637]

Significance

We demonstrate a novel approach for simultaneous detection of genomic rearrangements and enhancer activity in tumor biopsies. We identify novel mechanisms of enhancer-driven regulation of the oncogenes *MYC* and *BCL6*, and show that the *BCL6* locus can serve as an enhancer donor in an “enhancer hijacking” translocation.

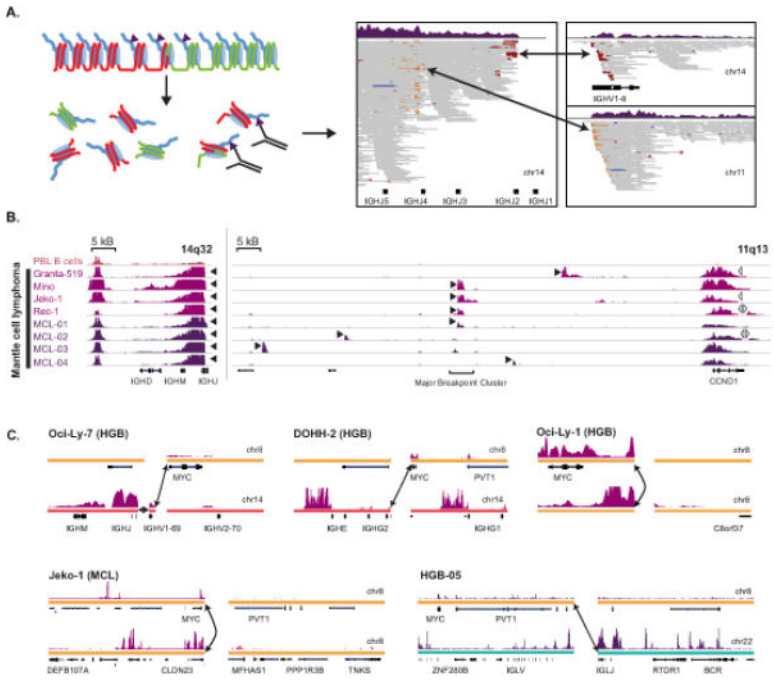

Figure 1.

Detection of rearrangements involving the *CCND1* and *MYC* loci by PEAR-ChIP. **A.** *Left* - Schematic depiction of a rearrangement between two chromosomes (red and green) with the breakpoint located in chromatin marked by H3K27ac (purple triangles). ChIP-Seq leads to isolation of H3K27ac-associated DNA, including enhancer-associated breakpoints. *Right* – Sequencing and alignment of ChIP DNA from case MCL-01 identifies read pairs at the ends of fragments containing the t(11;14) breakpoint (orange reads) and a physiological *IGH* VDJ recombination (red reads). **B.** Tracks showing H3K27ac signal in normal B cells (salmon), MCL cell lines (maroon) and MCL biopsies (dark purple) at the *IGH* and *CCND1* loci. *IGH-CCND1* rearrangement breakpoints detected by PEAR-ChIP are marked with black arrowheads. Also shown are breakpoints corresponding to intra-chromosomal deletions (paired open arrowheads) or large-scale rearrangements (single open arrowheads) affecting the *CCND1* 3'UTR. **C.** H3K27ac tracks and location of PEAR-ChIP-detected large-scale rearrangements (black arrows) involving the *MYC* locus.

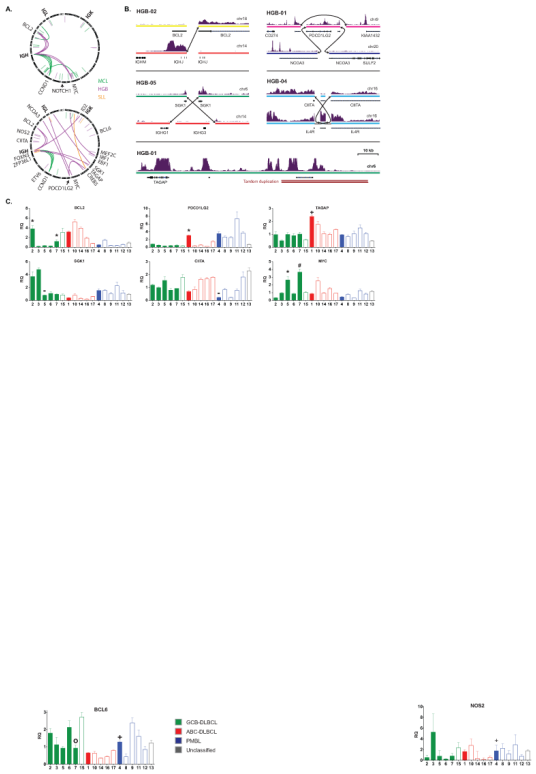

Figure 2.

Genome-wide rearrangement detection by PEAR-ChIP. **A.** Circos diagrams summarizing inter-chromosomal (dark shades) and intra-chromosomal (light shades) genomic rearrangements detected by H3K27ac PEAR-ChIP in 8 lymphoma cell lines (top) and 14 patient biopsies (bottom). Gene labels mark selected loci of interest. **B.** H3K27ac tracks and location of large-scale rearrangements (black arrows) detected by PEAR-ChIP at known oncogene (*BCL2* and *PDCD1LG2*) and tumor suppressor gene (*SGK1* and *CIITA*) loci, as well as a tandem duplication encompassing candidate enhancers upstream of *TAGAP*. Red bars link divergent read pairs spanning the tandem duplication. **C.** Normalized RNA expression (RQ = relative quantity) for genes affected by PEAR-ChIP-detected genomic lesions in HGB biopsies. Numbers at bottom denote the HGB sample name (e.g. “1” = HGB-01). Symbols indicate samples that contain a genomic lesion proximal to the measured gene (asterisk: inter-chromosomal rearrangement predicted to activate gene expression; minus sign: rearrangement predicted to inactivate gene expression; plus sign: enhancer tandem duplication). The pound sign denotes a FISH-detected rearrangement between the *MYC* and *BCL6* loci. Samples are color-coded by gene expression subtype as follows: green = GCB-DLBCL, red = ABC-DLBCL, blue = PMBL, gray = unclassified. Solid bars denote samples studied by PEAR-ChIP.

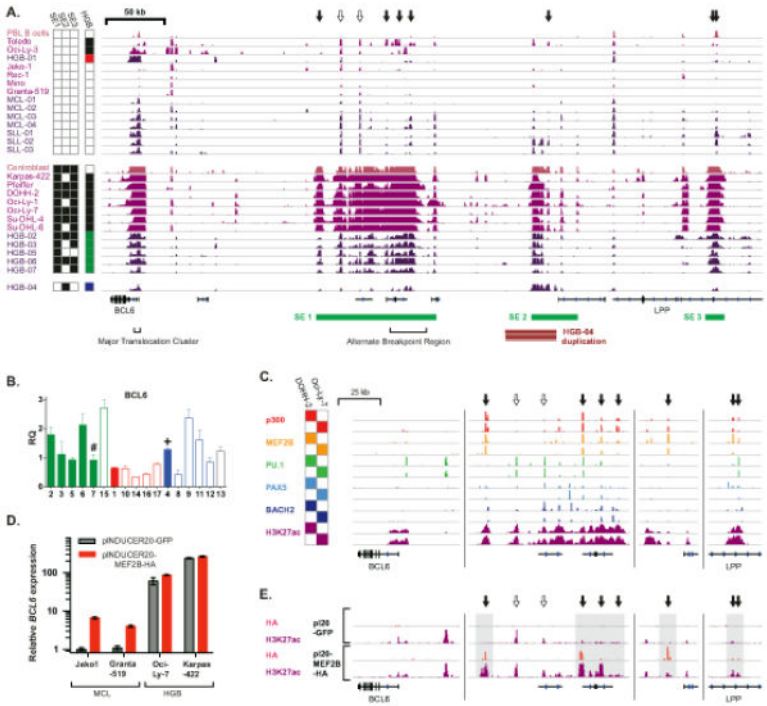

Figure 3.

Acetylation and rearrangement of *BCL6* locus enhancers. **A.** H3K27ac ChIP-Seq tracks across the *BCL6* locus in 29 B cell populations. Green bars at bottom indicate the median positions of detected super-enhancer regions. Black brackets indicate published breakpoint cluster regions. Read-pairs spanning the tandem duplication in HGB-04 are linked by red bars at bottom. The legend at left indicates the super-enhancers called in each population, as well as populations classified as HGB (red = ABC-DLBCL, green = GCB-DLBCL, blue = PMBL, black = HGB cell line). MEF2B-positive (black arrows) and selected MEF2B-negative TF binding sites (open arrows) are indicated, and correspond to positions indicated in (C). ChIP-seq coverage range is 0-5 fpm (fragments per million mapped fragments) for all tracks. **B.** Normalized RNA expression of *BCL6* in HGB biopsies. Samples are numbered and color-coded by subtype as in Figure 2C. Solid boxes indicate samples evaluated by PEAR-ChIP. Symbols indicate samples that contain a genomic lesion proximal to the measured gene (plus sign: enhancer tandem duplication, pound sign: FISH-detected rearrangement between the *MYC* and *BCL6* loci). **C.** ChIP-Seq tracks for p300, H3K27ac, and three TFs in two HGB cell lines at the *BCL6* promoter and super-enhancer regions. MEF2B-positive (black arrows) and selected MEF2B-negative TF binding sites (open arrows) are indicated and correspond to positions indicated in (A). ChIP-Seq coverage range is 0-15 fpm for H3K27ac. **D.** Relative *BCL6* expression in MCL and HGB cell lines stably transduced with pINDUCER-20 bearing a GFP or MEF2B-HA transgene, and harvested 48 hours after induction with 100 ng/ml doxycycline. **E**. ChIP-seq tracks for H3K27ac and HA-tag in Jeko-1 cells with induced expression of GFP or MEF2B-HA as in figure 4b. Genomic positions and arrows are identical to (C). ChIP-seq coverage range is 0-2.5 fpm for H3K27ac.

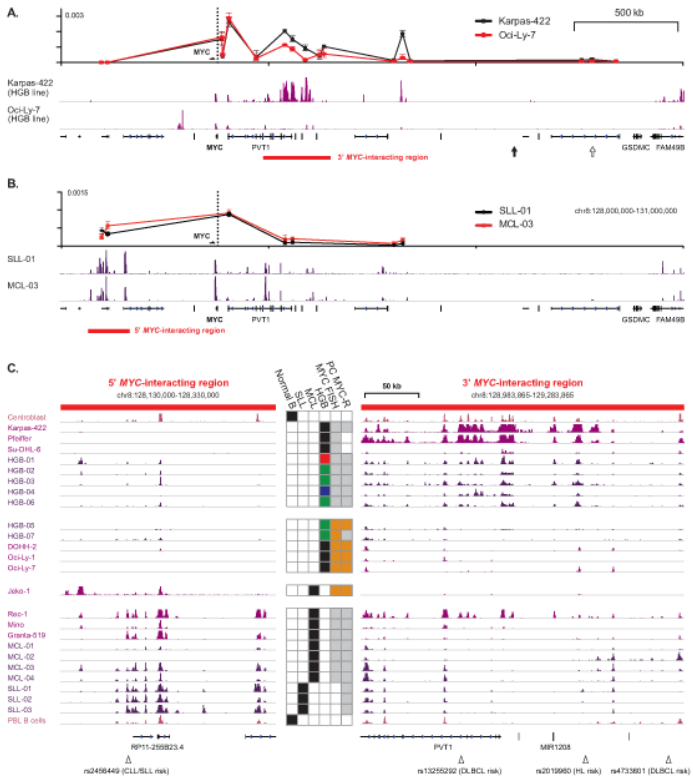

Figure 4.

Enhancer acetylation at native and rearranged *MYC* loci in B-cell lymphoma. **A.** Interaction of candidate *MYC* locus enhancer regions with the *MYC* promoter by chromatin conformation capture (3C) in HGB cell lines (top), and corresponding H3K27ac ChIP-Seq tracks (bottom). Red bar at bottom indicates 3' *MYC*-interacting region detailed in (C). Arrows indicate the positions of previously reported *MYC* enhancers in T cell leukemia (black arrow) (30) and myeloid leukemia (open arrow) (3). ChIP-seq coverage range is 0-10 fpm. **B.** Interaction of candidate *MYC* locus enhancer regions with the *MYC* promoter by chromatin conformation capture (3C) in MCL and SLL biopsies (top), and corresponding H3K27ac ChIP-Seq tracks (bottom). Red bar at bottom indicates 5' *MYC*-interacting region detailed in (C). ChIP-seq coverage range is 0-5 fpm. **C.** Detail of H3K27ac ChIP-seq tracks at *MYC*-interacting regions in B cell samples. Legend at center indicates lymphoma type (for HGB biopsies red = ABC-DLBCL, green = GCB-DLBCL, blue = PMBL) or normal B population, presence or absence of a *MYC* rearrangement by fluorescence *in situ* hybridization ("MYC FISH", orange: rearrangement, gray: not detected, white: not evaluated), and *MYC* rearrangement detection by PEAR-ChIP ("PC MYC-R"). Triangles at bottom indicate position and lymphoma subtype associations of single-nucleotide polymorphisms linked to hereditary risk for lymphoma in published GWAS studies. ChIP-seq coverage range is 0-5 fpm for all tracks.

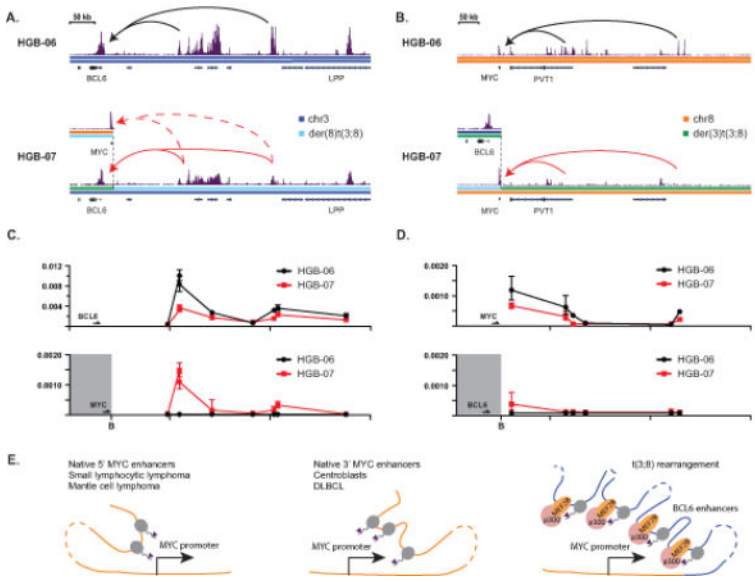

Figure 5.

A t(3;8)(q27;q24) rearrangement leads to *MYC* activation by *BCL6* enhancers. **A.** H3K27ac ChIP-Seq tracks at the *BCL6* locus for HGB-06 and HGB-07. The *MYC* promoter region is also shown for HGB-07, and a dashed black line connects the t(3;8) rearrangement breakpoints. Solid black (HGB-06) or red (HGB-07) arrows depict looping interactions on the native chromosome 3 as determined by 3C. Dashed red arrows depict looping interactions between *BCL6* enhancers and the *MYC* promoter in HGB-07, as determined by 3C. **B.** H3K27ac ChIP-Seq tracks at the *MYC* locus for HGB-06 and HGB-07. The *BCL6* promoter region is also shown for HGB-07, and a dashed black line connects the t(3;8) rearrangement breakpoints in HGB-07. Solid black (HGB-06) or red (HGB-07) arrows depict looping interactions on the native chromosome 8 as determined by 3C. **C.** 3C data for interactions between *BCL6* locus enhancers and the *BCL6* promoter (top) or *MYC* promoter (bottom) for HGB-06 and HGB-07. “B” indicates the position of the breakpoint junction on the der(8)t(3;8) in HGB-07. **D.** 3C data for interactions between *MYC* locus distal elements and the *MYC* promoter (top) or *BCL6* promoter (bottom) for HGB-06 and HGB-07. “B” indicates the position of the breakpoint junction on the der(3)t(3;8) in HGB-07. **E.** Schematic models of *MYC* promoter interactions with native and heterologous enhancers in B cell lymphomas.